Alluvial morphodynamics of low-slope bedrock reaches transporting non-uniform bed material

S. Jafarinik[1], and E. Viparelli[1]

[1]Civil and Environmental Engineering Department, University of South Carolina, Columbia, South Carolina, USA

Corresponding author: Enrica Viparelli (viparell@cec.sc.edu)

Key Points (at the end):

- We developed, implemented and tested a novel formulation for alluvial morphodynamics of bedrock reaches transporting non-uniform bed material
- Stable patterns of downstream coarsening are predicted upstream of a stable bedrock-alluvial transition
- In presence of sea level rise, a bedrock-alluvial transition migrates upstream and an alluvial-bedrock transition migrates downstream. The opposite is expected in case of sea level fall.

Abstract

Research on bedrock rivers primarily focused on bedrock incision and, to the best of our knowledge, morphodynamic models have not yet considered the variability of sediment grain size and the presence of small scale bedforms in low-slope (slope < 0.005) bedrock reaches. Further, very few models can quantify spatial and temporal changes in the fraction of channel bed covered with alluvium (alluvial cover) within these reaches. Here we present a novel formulation of alluvial morphodynamics of low-slope bedrock reaches transporting non-uniform bed material. The formulation is implemented in a one-dimensional model and validated against laboratory experiments on bedrock reaches downstream of stable alluvial-bedrock transitions, where the flow accelerates in space. The validated model is used to study the alluvial morphodynamics of bedrock reaches upstream of stable bedrock-alluvial transitions. Equilibrium results show that the interactions between flow, sediment transport and non-erodible bedrock surface result in a flow decelerating in the streamwise direction. The effects of this spatial flow deceleration are 1) a streamwise increase in alluvial cover, and 2) the formation of a pattern of downstream coarsening of bed surface sediment. We then investigated the effects of sea level rise/fall on the location of alluvial-bedrock and bedrock-alluvial transitions. In the case of sea level rise, alluvial-bedrock transitions migrate downstream and bedrock-alluvial transitions migrate upstream. Opposite migration directions are expected in the case of sea level fall.

1 Introduction

Bedrock reaches are frequently found in upland areas where the bed material is relatively coarse, is preferentially transported as bedload, and small scale bedforms such as dunes are absent [*Whipple et al.*, 2000; *Whipple and Tucker*, 2002; *Whipple*, 2004; *Sklar and Dietrich*, 2004; *Turowski et al.*, 2007; *Gasparini et al.*, 2007; *Chatanantavet and Parker*, 2008, 2009; *Lamb et al.*, 2008; *Lague*, 2010, 2014; *Hodge et al.*, 2011, 2016; *Chatanantavet et al.*, 2013; *Johnson*, 2014; *Zhang et al.*, 2015; *Inoue et al.*, 2014]. Recent field studies, however, show that bedrock reaches can also be found in lowland areas, where the bed material is relatively fine and small scale bedforms, such as dunes, are present. These reaches can be bounded by an upstream alluvial-bedrock transition and may also present a downstream bedrock-alluvial transition [*Nittrouer et al.*, 2011; *Shaw et al.*, 2013; *Shaw and Mohrig*, 2014].

Viparelli et al. [2015] demonstrated that low-slope bedrock rivers, i.e. rivers with bedrock and alluvial slopes milder than 0.005 [*Chatanantavet and Parker*, 2008], can reach an equilibrium configuration in the absence of bedrock incision, sea level rise and subsidence. At equilibrium, the location of alluvial-bedrock and bedrock-alluvial transitions does not change in space and in time [*Viparelli et al.*, 2015].

Equilibrium is a condition in which bed elevation averaged over time scales that are long compared to the time scales of bedform migration [*Blom et al.*, 2006] and bedload transport [*Wong et al.*, 2007] is constant in time [*Anderson et al*., 1975]. If base level, formative discharge and sediment supply are constant in time, in equilibrium alluvial reaches the bed material load is everywhere equal to the sediment supply and to the transport capacity of the flow, [*Parker*, 2004]. If abrasion is not accounted for, equilibrium grain size distributions of bed material load and of bed surface sediment do not change in space and time [*Blom et al.*, 2016]. In particular,

79 the grain size distribution of the bed material load is equal to the grain size distribution of the
80 sediment supply, and the grain size distribution of the bed surface sediment is generally coarser
81 than the grain size distribution of the sediment supply to regulate the different mobility of coarse
82 and fine grains [*Blom et al.*, 2016 and references therein].

83 In low-slope bedrock channels transporting sand as bed material, equilibrium is
84 characterized by steady and not uniform flow conditions. Spatial changes in mean flow velocity
85 are associated with spatial changes in alluvial cover, i.e. the areal fraction of bed surface covered
86 with alluvium [*Viparelli et al.*, 2015]. In particular, in case of flow acceleration (e.g. downstream
87 of a stable alluvial-bedrock transition) the alluvial cover decreases in the streamwise direction,
88 and the opposite is observed in the case of spatial flow deceleration (e.g. upstream of a stable
89 bedrock-alluvial transition) [*Viparelli et al.*, 2015]. The conservation of channel bed material
90 imposes that at equilibrium the bed material load is equal to the sediment supply. In equilibrium
91 bedrock rivers, spatial changes of bed material transport capacity are balanced by streamwise
92 changes in alluvial cover, which limit sediment availability so that the bed material load is
93 everywhere equal to the sediment supply [*Viparelli et al.*, 2015].

94 Laboratory experiments on equilibrium low-slope bedrock rivers transporting non-
95 uniform sand showed that, as the flow spatially accelerates downstream of a stable alluvial-
96 bedrock transition, flow resistances decrease in the streamwise direction due to downstream
97 fining of the bed surface sediment (reduction of skin friction), streamwise decrease in bedform
98 height (reduction of form drag), or a combination of the two [*Jafarinik et al.*, 2019]. Thus, in
99 response to flow acceleration/deceleration 1) spatial variations in bedform height and wavelength
100 may result in a spatially changing form drag, and 2) stable patterns of downstream fining or
101 coarsening of bed surface sediment may form [*Jafarinik et al.*, 2019].

To the best of our knowledge, models of alluvial morphodynamics of bedrock rivers do not account for the non-uniformity of the bed material grain size and for changes in flow resistances associated with a spatial change in the bedform geometry and grain size distribution of the bed surface sediment [*Lague,* 2010; *Zhang et al*., 2015; *Johnson,* 2014; *Viparelli et al*., 2015]. Here we present a novel formulation for the alluvial morphopdynamics of bedrock rivers that accounts for the non-uniformity of the bed material grain size and the presence of small scale bedforms. We implemented the formulation in a one-dimensional model and validate the model against experimental results [*Jafarinik et al.*, 2019]. We apply the validated model to study equilibrium of a low-slope bedrock reach with a stable bedrock-alluvial transition, and the morphodynamics of a bedrock reach with variable downstream water level. Model applicability to steep bedrock rivers (bedrock slope greater than 0.005), where equilibrium conditions may be initial-condition dependent [*Chatanantavet and Parker*, 2008], is also briefly discussed.

2 Model formulation

The model formulation is not site specific and can be applied to either field or laboratory scales. Application-specific relations to compute flow resistances and bed material transport capacity should be chosen based on problem characteristics. Model governing equations are the one-dimensional shallow water equations of mass and momentum conservation for open channel flow, the grain size specific equation of conservation of bed material, and the equation of conservation of total (summed over all the grain sizes) bed material.

The following assumptions and approximations are introduced to simplify the problem:

1. The ratio between the volumetric bed material load and the flow discharge is assumed to be orders of magnitude smaller than one, so that the quasi-steady approximation holds for the flow [*De Vries*, 1965];

2. The bedrock is assumed to be non-erodible. The extension of the formulation to erodible bedrock surfaces is relatively straightforward [e.g. *Sklar and Dietrich*, 2004; *Lamb et al.*, 2008];

3. A procedure to account for different roughness between the smooth sidewalls and the rough bed is implemented for lab scale applications [*Vanoni and Brooks*, 1957];

4. When applied at field scale, the model describes the long-term evolution of the river channel. It does not account for the exchange of sediment between the channel and the floodplain due to for example overbank deposition of suspended sediment, channel migration or widening [e.g. *Viparelli et al.*, 2011; *Lauer et al.*, 2016];

5. Base level is assumed constant, but the modification of the formulation to account for subsidence, uplift or sea level rise is straightforward, as shown in the discussion section of this manuscript;

6. The bed material is preferentially transported as bedload. The implementation of grain size specific suspended load calculations is also relatively simple;

7. The cross section is assumed to be rectangular with uniform width that does not change in time. The extension to the case of a spatially varying cross section with geometry that does not change in time is cumbersome but not complex [*Viparelli et al.*, 2015]; and

8. The active layer approximation is used to model the exchange of bed material between the mobile bed and the bedload [*Hirano*, 1971; *Parker*, 1991a, b]

144 *2.1 Model geometry*

145 The schematic longitudinal profile of the modeled system is presented in Figure 1, where
146 the black line represents the deepest portion of the bedrock surface with elevation η_b, and slope
147 S_b [*Zhang et al.*, 2015], the grey line denotes the locally averaged elevation of the alluvial bed η
148 [*Parker et al*., 2000; *Zhang et al*., 2015] and ζ is the downstream water surface elevation. The
149 dashed line at elevation η_b+L_{ac} identifies the minimum elevation of the alluvial bed such that in-
150 channel sediment transport processes are not affected by the underlying bedrock [*Viparelli et al.*,
151 2015]. In other words, L_{ac} represents the minimum thickness of alluvial cover for complete
152 channel bed alluviation. In a bedrock reach the elevation of the alluvial bed, η, is smaller than
153 η_b+L_{ac}, in an alluvial reach $\eta > \eta_b + L_{ac}, \eta = \eta_b + L_{ac}$ corresponds to the location of a bedrock-
154 alluvial or an alluvial-bedrock transition [*Viparelli et al.*, 2015].

155

156 *2.2 Flow equations*

157 The one-dimensional shallow water equations of mass and momentum conservation for
158 open channel flow are presented in equations (1) and (2) [*Chaudhry*, 2007].

$$\frac{\partial H}{\partial t} + \frac{\partial UH}{\partial x} = 0 \tag{1}$$

$$\frac{\partial U}{\partial t} + g\frac{\partial}{\partial x}\left(\frac{U^2}{2g} + H\right) = g(S - S_f) \tag{2}$$

159 where x and t respectively represent streamwise and temporal coordinates, U and H respectively
160 denote the flow depth and the mean flow velocity, g is the acceleration of gravity, S is the
161 channel bed slope defined herein as the slope of the alluvial bed $S = -\partial\eta/\partial x$, and S_f denotes the
162 friction slope. Equations (1) and (2) are simplified with the quasi-steady approximation [*De*
163 *Vries*, 1965], i.e. time derivatives are dropped and equations (1) and (2) reduce to

$$q_w = UH \tag{3}$$

$$g\frac{\partial}{\partial x}\left(\frac{U^2}{2g} + H\right) = g(S_o - S_f) \tag{4}$$

where q_w is the flow discharge per unit channel width. Substituting equation (3) into equation (4), the backwater equation for one-dimensional gradually varied steady flow is obtained

$$\frac{\partial H}{\partial x} = \frac{S - S_f}{1 - Fr^2} \tag{5}$$

where Fr is the Froude number defined as $U/\sqrt{gH}$ and S_f represents the friction slope which is defined as

$$S_f = \frac{C_f U^2}{gR_h} \tag{6}$$

where C_f is a non-dimensional friction coefficient and R_h is the hydraulic radius. The general friction coefficient formulation used herein is the Manning-Strickler formulation as follows.

$$C_f^{-1/2} = \alpha_r\left(\frac{R_h}{k}\right)^{\frac{1}{6}} \tag{7}$$

where α_r is a model parameter equal to 8.1 [*Parker*, 2004] and k denotes the roughness height. The calculation of C_f depends on the problem of interest.

Equation (5) is integrated with a first order, finite difference scheme in the upstream direction with downstream boundary condition expressed in terms of known downstream water level, as appropriate in the case of subcritical flows.

2.3 Conservation of bed material

To account for the non-uniformity of the bed material grain size, sediment fluxes between the alluvial bed and the bed material load are modeled with the aid of the active layer

179 approximation. In active layer-based models, the deposit is divided in two regions, the active
180 layer and the substrate. The active layer represents the topmost part of the deposit that interacts
181 with the bed material load. The substrate is the part of the deposit underneath the active layer
182 with grain size distribution that can change in space, i.e. in the vertical and streamwise direction
183 [*Parker et al.*, 2000].

184 The definition of the active layer thickness L_a is not straightforward and relies on
185 observations. In gravel bed rivers, where small scale bedforms such as dunes are generally
186 absent [*Parker and Klingemann*, 1982], the active layer thickness scales with the coarsest grain
187 sizes of the bed surface material. In sand bed rivers, where small scale bedforms such as dunes
188 are generally present, the thickness of the active layer is hard to define and it generally scales
189 with bedform height [*Blom*, 2008].

190 In active layer-based models, two equations of conservation of bed material are solved: 1)
191 the equation of conservation of total, i.e., summed over all the grain sizes, bed material to
192 compute the changes in mean bed elevation, and 2) the grain size specific equation of
193 conservation of bed material to compute spatiotemporal changes of active layer sediment size
194 distribution. In the continuing of this section we illustrate how equations of conservation of
195 alluvial bed material can be used to model the alluvial morphodynamics of bedrock rivers.

196

197 i. *Equation of conservation of bed material summed over all the grain sizes*

198 The equation of conservation of total bed material in bedrock reaches takes the form
199 [*Zhang et al.*, 2015]

$$(1-\lambda_p)p_c\frac{\partial \eta}{\partial t}=-\frac{\partial q_{bT}}{\partial x} \quad (8)$$

where λ_p denotes the bulk porosity of the alluvial deposit, q_{bT} is the total volumetric bed material load per unit channel width and p_c represents the alluvial cover defined as the areal fraction of bed that is covered with alluvium [*Nelson and Seminara*, 2012; *Inoue et al.* 2014 and *Johnson*, 2014]. The total volumetric bed material load per unit channel width is equal to the total volumetric bed material transport capacity q_{bTc} computed with an empirical relation such as *Ashida and Michiue* [1972] or *Wilcock and Crowe* [2003] multiplied by p_c [*Sklar and Dietrich*, 2004].

ii. *Grain size specific equation of conservation of bed material*

If the density of the bed material does not vary from one characteristic grain size to the other, the one-dimensional, grain size specific conservation of bed material can be phrased as follows: the time rate of change of bed material with characteristic grain size D_i in a control volume is equal to the net influx of bed material with grain size D_i. In bedload dominated rivers, the grain size specific equation of conservation of bed material takes the following form (see *Zhang et al*. [2015] for the derivation in the case of uniform sediment)

$$(1-\lambda_p)\frac{\partial}{\partial t}\int_{\eta_b}^{\eta} p_b f_i dz=-\frac{\partial q_{bi}}{\partial x} \quad (9)$$

where z denotes an upward oriented vertical coordinate, p_b represents the probability that a point at elevation z relative to an arbitrary datum is not bedrock [*Zhang et al*., 2015], f_i is the volume fraction content of bed material with characteristic grain size D_i at elevation z and q_{bi} is the bedload transport rate of bed material particles with characteristic grain size D_i. In general, f_i

varies in space (x and z) and in time. In a fully alluvial system, the lower limit of integration in equation (12) refers to a point very deep in the alluvial deposit [*Parker et al.*, 2000]. Here, as in *Zhang et al.* [2015], the lower limit of integration η_b corresponds to the elevation of the *bottom of the bedrock surface*, i.e. a point where $p_b = 0.05$. The grain size specific bedload transport rate, q_{bi} is equal to the product of the grain size specific bedload transport capacity q_{bic} and p_c. The sum of q_{bi} over all the grain size fractions is equal to q_{bT}.

The active layer approximation [*Hirano*, 1971; *Parker*, 1991a, b] is used to solve the integral on the left-hand side of equation (9). The alluvial deposit is thus divided in two parts, the active layer and the substrate. The active layer is a relatively thin, mixed layer on the topmost part of the deposit whose sediment size distribution can change in time due to the exchange of sediment with the bedload transport. The substrate is the deposit between the bedrock surface and the active layer. Substrate sediment size distribution can change in x and z but not in time, unless η changes in time. In other words, the volume fraction content of sediment with characteristic grain size D_i in the active layer F_i can change in the streamwise direction and in time, and the volume fraction content of substrate sediment in the generic grain size range f_i' changes in time when the channel bed aggrades or degrades.

If the active layer-substrate interface elevation is higher than the elevation of the bottom of the bedrock surface, $(\eta - L_a) \geq \eta_b$, we express the left hand side of equation (9) as the sum of the integral of $p_b f_i$ in the substrate (between η_b and η-L_a) and in the active layer (between η- L_a and η) with L_a denoting the active layer thickness in the case of a fully alluvial system, equation (10a). If the active layer-substrate interface elevation is below the bottom of the bedrock surface, $(\eta - L_a) < \eta_b$, the left-hand side of equation (9) is equal to the integral of $p_b f_i$ between η_b and η, equation (10b). The integral of equation (9) thus takes the form

$$\frac{\partial}{\partial t}\int_{\eta_b}^{\eta} p_b f_i dz = \frac{\partial}{\partial t}\left(\int_{\eta_b}^{\eta-L_a} p_b f_i' dz + \int_{\eta-L_a}^{\eta} p_b F_i dz\right) \quad \text{if } (\eta - L_a) \geq \eta_b \tag{10a}$$

$$\frac{\partial}{\partial t}\int_{\eta_b}^{\eta} p_b f_i dz = \frac{\partial}{\partial t}\int_{\eta_b}^{\eta} p_b F_i dz \quad \text{if } (\eta - L_a) < \eta_b \tag{10b}$$

)

In the absence of bedrock incision, subsidence and uplift, the limits of integration that are a function of time are η and η - L_a. The Leibnitz rule is thus applied to compute the derivative of the first integral on the right-hand side of equation (10a) as

$$\frac{\partial}{\partial t}\int_{\eta_b}^{\eta-L_a} p_b f_i^{'} dz = \int_{\eta_b}^{\eta-L_a} \frac{\partial(p_b f_i^{'})}{\partial t} dz + \left(p_b f_i^{'}\right)|_{z=\eta-L_a} \frac{\partial}{\partial t}(\eta - L_a) = p_{bI} f_{Ii} \frac{\partial}{\partial t}(\eta - L_a) \tag{11}$$

where f_{Ii} denotes the volume fraction content of bed material with grain size D_i at the active layer-substrate interface and p_{bI} is probability that a point at the active layer-substrate interface ($z = \eta - L_a$) is either in water or in alluvium.

The derivative of the second integral on the right-hand side of equations (10a) and (10b) is easy to compute because the active layer is a mixed layer (F_i does not vary in the z direction). Further, recalling that η is the locally averaged elevation of the alluvium, the integral of p_b between ($\eta - L_a$) and η represents the volume of sediment per unit bed area in the active layer, i.e., the average thickness of the active layer, $L_{a,av}$ in the bedrock reach. For the same reason, the integral in equation (13b) is equal to $F_i L_{a,av}$.

In an alluvial system $p_b = 1$, $L_{a,av} = L_a$ and the volume of active layer sediment per unit bed area with grain size D_i is equal to $F_i L_a$. In bedrock reaches, $L_{a,av} < L_a$ due to the presence of exposed bedrock. Substituting equations (10) and (11) in equations (9), the grain size specific equation of conservation of bed material takes the form

$$(1-\lambda_p)\left[p_{bI}f_{Ii}\frac{\partial}{\partial t}(\eta - L_a) + \frac{\partial}{\partial t}\left(F_i L_{a,av}\right)\right] = -\frac{\partial q_{bi}}{\partial x} \quad (12)$$

When $(\eta - L_a) < \eta_b$, the probability that a point at elevation $(\eta - L_a)$ is either in water or in alluvium, p_{bI}, is equal to zero and consequently the sediment flux between the active layer and the substrate, i.e. the first term in the left-hand side of equation (12), is also equal to zero.

When $(\eta - L_a) \geq \eta_b$, the volume fraction content of bed material at the active layer-substrate interface, f_{Ii}, is computed with the *Hoey and Ferguson* [1994] formulation, as

$$f_{Ii} = \begin{cases} f_i'|_{z=\eta-L_a}, & \frac{\partial \eta}{\partial t} < 0 \\ \alpha F_i + (1-\alpha) f_{load,i}, & \frac{\partial \eta}{\partial t} \geq 0 \end{cases} \quad (13)$$

where $0<\alpha<1$ and $f_{load,i}$ is the volume fraction content of bed material with characteristic grain size D_i in bedload transport q_{bi}/q_{bT}. To determine p_{bI}, i.e. the probability that a point at elevation $(\eta - L_a)$ is in alluvium or water, we follow *Zhang et al*. [2015] and *Viparelli et al*. [2015]:

1) we characterize the local variation in bedrock elevation in terms of a minimum thickness of alluvial cover for complete channel bed alluviation L_{ac}. In other words, L_{ac} represents the minimum vertical distance between the top of the alluvium and the bottom of the bedrock surface such that in-channel sediment transport processes are not influenced by the bedrock surface (see Figure 1) [*Viparelli et al.*, 2015];

2) we recall that $(\eta - \eta_b)$ represents the elevation difference between the locally averaged top of alluvium and the bottom of the bedrock surface and that $[1 - p_b(z)]$ represents the probability that a point at elevation z is bedrock [*Zhang et al*., 2015]. Changes in bed level due to bedload transport and bedform migration [*Parker et al.*, 2000; *Blom et al.*,

2003; *Wong et al.*, 2007] are not modeled, thus if $z \leq \eta$, $p_b(z)$ represents the probability that a point at elevation z is in alluvium, and if $z > \eta$, $p_b(z)$ represents the probability that a point at elevation z is in water; consequently

3) the cover fraction p_c at elevation z, with $\eta_b < z \leq \eta$ is equal to p_b, i.e. $p_c[(z - \eta_b)/L_{ac}] = p_b(z)$ [*Zhang et al*., 2015].

2.4 The flow of the calculation

The modeled domain is divided into N reaches bounded by N+1 computational nodes. Initial conditions are the longitudinal profile of the alluvial bed, the grain size distributions of the active layer and of the substrate. Model boundary conditions are assigned in terms of a longitudinal profile of the bottom of the bedrock surface, flow rate, sediment feed rate and grain size distribution, and downstream water surface elevation. It is important to mention here that in the simulation presented below the grain size distribution of the substrate is assumed to be equal to the grain size distribution of the sediment feed.

The flow is assumed to be Froude subcritical and equation (5) is integrated in the upstream direction. Bed shear stresses are estimated in each computational node, and bedload transport rates are computed with a surface-based formulation modified to account for the presence of exposed bedrock [*Jafarinik et al.*, 2019]. The equation of conservation of total bed material (equation 8) is integrated to estimate the time rate of change of mean alluvial bed elevation, and finally the grain size specific equation of conservation of active layer sediment (equation 12) is integrated to update the grain size distribution of active layer sediment. Calculations are either repeated for a user specified duration of simulated time, or until the

297 system reaches equilibrium, i.e. when the alluvial bed elevation does not change in time and the
298 bedload transport rate becomes equal to the upstream sediment supply in each node.

299

300 **3 Overview of the laboratory experiments**

301 The morphodynamic framework presented above is implemented in a one-dimensional
302 model and validated against laboratory experiments on equilibrium mixed bedrock channels
303 downstream of an alluvial-bedrock transition [*Jafarinik et al.*, 2019]. *Jafarinik et al.* [2019]
304 performed four pairs of experiments to compare equilibrium conditions in fully alluvial and
305 mixed bedrock-alluvial reaches subject to the same flow rate and sediment supply. The
306 experiments were performed in a 6 m long and 0.19 m wide sediment feed flume with constant
307 feed rate, flow rate and water surface base level. The model bedrock was a sheet of marine
308 plywood and sand grains were glued to the plywood to create a somewhat rough boundary. The
309 grain size distribution of the sediment types used in the experiments is presented in Figure 2,
310 where the black line is the grain size distribution of the uniform sand with geometric mean
311 diameter D_g = 1.11 mm and geometric standard deviation σ_g = 1.44 mm and the grey line is the
312 grain size distribution of the nonuniform sand with geometric mean diameter D_g = 0.87 mm and
313 geometric standard deviation σ_g = 1.69 mm. At equilibrium, time series of bed and water surface
314 elevation were measured with ultrasonic probes, alluvial cover and flow characteristics averaged
315 over a series of bedforms were computed. Sediment samples were then collected to measure the
316 grain size distribution of the bed surface, defined as the entire thickness of the alluvial layer in
317 the bedrock reaches [*Jafarinik et al.*, 2019].

318 Prior to model verification, which is a necessary step to determine if the morphodynamic
319 formulation presented above is adequate to simulate the alluvial morphodynamics of low-slope

bedrock rivers, sub-models to predict alluvial cover [*Viparelli et al.*, 2015], bedform height, bedload transport rates and flow resistances have to be determined or validated using the experimental data. If one of these sub-models does not adequately reproduce the experimental observations, the proposed morphodynamic formulation cannot be verified against the experimental results because the differences between numerical predictions and experimental data will be (at least) partially due to the use of an inadequate sub-model [*Viparelli et al*., 2010].

3.1 Alluvial cover

In the model simulations the alluvial cover is computed with the linear relation used by *Viparelli et al*. [2015] which has not been compared with laboratory or field data

$$p_c = \begin{cases} 0.05 + 0.95\dfrac{\eta - \eta_b}{L_{ac}} & if \quad \dfrac{\eta - \eta_b}{L_{ac}} \leq 1 \\ 1 & if \quad \dfrac{\eta - \eta_b}{L_{ac}} > 1 \end{cases} \qquad (14)$$

Equation (14) is validated against the *Jafarinik et al.* [2019] experiments. The average thickness of alluvial cover L_{ac} in the equation is assumed to be equal to $1.5\sigma_a$, with σ_a being the standard deviation of bed elevation changes over time scales that are short compared to the time scales of channel bed aggradation/degradation. The subscript *a* indicates that the standard deviation of bed elevations is determined in fully alluvial reaches subject to the same flow rate and sediment supply as the bedrock reach of interest [*Jafarinik et al.*, 2019]. *Tuijnder et al.* [2009] performed experiments on sand dunes migrating on an immobile gravel layer and showed that the interaction between the gravel layer and the bedforms became negligible when the average thickness of the alluvial layer was equal or greater than ~1.5 times the bedform height.

The comparison between model predictions and experimental results is presented in Figure 3, where the dots represent the experimental points, the black line is equation (14) and the dashed lines indicate ±25% around the predicted value. The difference between predictions and laboratory measurements is larger than 25% in only 3 cases corresponding to ~10% of the experimental points. Thus, equation (14) reasonably reproduces the experimental observations and can be used to predict the alluvial cover of the *Jafarinik et al.* [2019] experiments in a one-dimensional model of alluvial morphodynamics of bedrock rivers.

3.2 Bedform amplitude predictor

The active layer thickness in presence of small scale bedforms generally scales with bedform amplitude [*Blom*, 2008]. In bedrock reaches bedform amplitude is generally smaller than in alluvial reaches subject to the same flow rate and sediment supply [*Tuijnder et al*., 2009; *Jafarinik et al.*, 2019]. In addition, bedform amplitude may also change in space as a consequence of the non-uniformity of the flow on the bedrock reach [*Jafarinik et al.*, 2019].

Predictive relations linking bedform amplitude in a bedrock reach with flow characteristics are, to the best of our knowledge, not available in the literature. Here we use the standard deviation of time series of elevations at equilibrium σ as a measure of bedform amplitude [*Jafarinik et al.*, 2019]. To estimate σ we use *Jafarinik et al.* [2019] data and we find a linear regression between the Froude number of the flow and the non-dimensional standard deviation of bed elevations σ/D_{sg} with D_{sg} being the geometric mean size of the bed surface sediment

$$\frac{\sigma}{D_{sg}} = -25.97Fr + 23.5 \quad (15)$$

Experimental measurements and equation (15) are presented in Figure 4, where the dots are the experimental points and the line is equation (15). The ratio σ/D_{sg} decreases with increasing Froude number, i.e. the dune height decreases as the flow accelerates in the streamwise direction downstream of a stable alluvial-bedrock transition. Due to the limited number or experimental data, as well as the value of R^2 equal to 0.65, equation (15) can be used here for model verification at laboratory scale but should be used with extreme care (if at all) to predict bedform characteristics in other experimental facilities or at field scales.

The active layer thickness, L_a, is set equal to $n_\sigma\sigma$ to capture the reduction in active layer thickness in equilibrium bedrock reaches [*Jafarinik et al.*, 2019]. In the simulations presented below n_σ =1. If the probability density function of bed elevations is approximated with a Gaussian distribution [*Singh et al*., 2011], ~ 68% of the changes in bed elevation are contained in an interval of amplitude σ around the mean bed level [*Jafarinik et al.*, 2019].

3.3 Calculation of the flow resistances

The experiments presented in *Jafarinik et al.*, [2019] were performed in a 0.19 m wide laboratory flume, thus for a proper calculation of the flow resistances and of the shear stresses acting on the channel bed, the different roughness between the rough bed and the smooth flume sidewalls must be accounted for [*Vanoni and Brooks*, 1957]. Hence, we implemented the *Vanoni and Brooks* [1957] sidewall correction procedure as described in *Chiew and Parker* [1994] to estimate flow resistances and bed shear stress from laboratory data collected in narrow flumes. It suffices to say here that to compute the flow resistances associated with the presence

of a granular bed in a narrow flume with smooth sidewalls, the cross section has to be divided in two regions, the bed region, where the flow is primarily impacted by the presence of the rough bed, and the wall region where flow characteristics are primarily controlled by the smooth sidewalls [see *Viparelli et al.*, 2014 for details on the implementation].

Here we use the subscript b to refer to sidewall corrected values, i.e. values characteristics of the granular bed. Equation (7) can thus be rewritten as

$$C_{fb}{}^{-1/2} = \alpha_r \left(\frac{R_{h,b}}{k_c}\right)^{\frac{1}{6}} \tag{16}$$

where $R_{h,b}$ is the hydraulic radius in the bed region [*Chiew and Parker*, 1994] and k_c is a cross-sectionally averaged composite roughness height that accounts for 3 different types of flow resistances, 1) flow resistances associated with the presence of a granular bed (skin friction), 2) flow resistances associated with the presence of bedforms (form drag) and 3) flow resistances associated with irregularities of the bedrock surface.

To implement equation (16) in the morphodynamic model presented above, we need a predictive formula for k_c. Here, due to the lack of experimental data on bedform geometry in bedrock reaches, we use an exponential regression on the experimental data by *Jafarinik et al.* [2019] presented in Figure 5.

$$\frac{k_c}{D_{s90}} = 0.17 e^{0.35\frac{\sigma}{D_{sg}}} \tag{17}$$

where D_{s90} is the diameter of the bed surface sediment such that 90% of the sediment is finer and σ/D_{sg} is computed with equation (15). It is important to recognize that equation (17) is experiment-specific and should not be regarded as a general formulation applicable to other cases.

Form drag does not contribute to bedload transport [e.g. *Engelund and Hansen*, 1967], thus the cross-sectionally averaged bed shear stress associated with skin friction has to be computed for bedload transport calculation. We consider an ideal flow over a plane bed with the same energy gradient S_f and mean flow velocity U as the flow in presence of bedforms [see *Parker*, 2004 for the case of alluvial beds]. The bed shear stress associated with skin friction is thus equal to $\rho C_{f,s} U^2$ with ρ being the water density and $C_{f,s}$ the skin friction coefficient. To compute $C_{f,s}$ with equation (7), the cross-sectionally averaged roughness height associated with skin friction $k_{s,c}$ has to be determined. In the formulation presented herein $k_{s,c}$ is equal to

$$k_{s,c} = p_c k_{s,a} + (1 - p_c) k_{s,b} \tag{18}$$

where $k_{s,a}$ and $k_{s,b}$ are the roughness heights associated with skin friction for the alluvium and for the bedrock respectively. In the model simulations presented below $k_{s,a}$ is assumed to be $2D_{s90}$ and $k_{s,b}$ is equal to the roughness height of the model bedrock in *Jafarinik et al*. [2019] experiment i.e. 0.1 mm. Equation (7) is thus rewritten as

$$C_{f,s}^{-1/2} = \alpha_r \left(\frac{R_{h,s}}{k_{s,c}}\right)^{\frac{1}{6}} \tag{19}$$

where $R_{h,s}$ is the hydraulic radius of the ideal flow. Unknowns in equation (19) are $C_{f,s}$ and $R_{h,s}$, thus a second equation is needed to solve the problem. The condition of equal friction slope for the real and the ideal flows is expressed with the aid of equation (6) as

$$\frac{C_f}{R_h} = \frac{C_{f,s}}{R_{h,s}} \tag{20}$$

Equations (19) and (20) are iteratively solved to determine $C_{f,s}$ and $R_{h,s}$.

3.4 Bedload transport formulation

The Ashida and Michiue bedload transport relation is used for model verification because it reasonably reproduces total and grain size specific sediment fluxes in the experiments with exposed bedrock [*Jafarinik et al.*, 2019]. When the non-uniformity of the bed material grain size is accounted for in models of river morphodynamics, the grain size distribution of the bed material is described in terms of M characteristic grain size diameters D_i. The Ashida and Michiue bedload relation for mixtures of sediment particles differing in size takes the form [*Parker*, 2008]

$$q_{bi}^{*} = 17\left(\tau_{bsi}^{*} - \tau_{refi}^{*}\right)\left(\sqrt{\tau_{bsi}^{*}} - \sqrt{\tau_{refi}^{*}}\right) \tag{21}$$

where q_{bi}^{*} is the grain size specific Einstein number, i.e. the non-dimensional volumetric bed material load per unit channel width; τ_{bsi}^{*} denotes the grain size specific Shields number associated with skin friction, i.e. the non-dimensional bed shear stress associated with skin friction; and τ_{refi}^{*} is the grain size specific reference Shields number for the initiation of significant bedload transport of particles with characteristic grain size D_i [*Parker*, 2008]. The grain size specific Einstein number and the grain size specific Shields number associated with skin friction are respectively defined in equations (22) and (23) as

$$q_{bi}^{*} = \frac{q_{bi}}{\sqrt{RgD_i}D_i p_c F_i} \tag{22}$$

$$\tau_{bsi}^{*} = \frac{\tau_{bs}}{\rho R g D_i} \tag{23}$$

where R denotes submerged specific gravity of the sediment and τ_{bs} is the bed shear stress associated with skin friction.

The grain size specific reference value of the Shields number of equation (21) is computed with the hiding/exposure function [*Parker*, 2008]

$$\frac{\tau^*_{refi}}{\tau^*_{srg}} = \begin{cases} 0.843\left(\frac{D_i}{D_{sg}}\right)^{-1} & for\ \frac{D_i}{D_{sg}} \leq 0.4 \\ \left[\frac{\log(19)}{\log(19\frac{D_i}{D_{sg}})}\right]^2 & for\ \frac{D_i}{D_{sg}} > 0.4 \end{cases} \quad (24)$$

where τ^*_{srg} is a reference value equal to 0.05 [*Parker*, 2008].

4 Model validation

Model validation is performed in two phases, we first compare model results and alluvial equilibrium experiments to verify that the present formulation is able to reproduce the equilibrium characteristics of a fully alluvial system. We then compare experimental measurements and numerical predictions of equilibrium conditions in the experiments with bedrock reaches. Model boundary conditions for the validation runs are summarized in Table 1 in terms of flow rate, sediment feed rate, sediment type (uniform or non-uniform sand of Figure 2), downstream water surface base level (ξ_d), alluvial equilibrium water depth (H_o) and the reach type, i.e., alluvial or with exposed bedrock.

4.1 Alluvial equilibrium runs

The comparison between measured and modeled alluvial equilibrium water depth, bed slope, bed shear stress associated with skin friction and the geometric mean diameter of the surface material are respectively presented in Figure 6 panels a-d. In the plots of Figure 6 the numerical equilibrium values are on the horizontal axes and the measured values are on the

vertical axes. The continuous black lines denote perfect agreement between numerical predictions and experimental observations. Each black diamond represents an alluvial equilibrium experiment (odd runs in Table 1). Dashed grey lines represent error bounds around the line of perfect agreement. Numerical predictions of water depth and flow velocity are within 20% error from the experimental observations. Numerical predictions of bed slopes are within 30% error of the measured value. The comparison between numerical and experimental predictions of shear stresses associated with skin friction and geometric mean diameter of the surface material are also within 30% and 10% error respectively. Therefore, Figure 6 shows that, given the model simplifications and the use of empirical relations to compute the flow resistances and the sediment fluxes, the proposed model is able to capture the experimental observations with errors that are comparable with those of other one-dimensional, active layer-based models of alluvial morphodynamics that account for the non-uniformity of the bed material [e.g. *Viparelli et al.*, 2010; *Viparelli et al.*, 2014].

4.2 Equilibrium runs with a bedrock reach

The comparison between numerical predictions and experimental measurements is presented in Figure 7 in terms of water surface and bed elevations (panels a, c, f and i), alluvial cover (panels b, d, g, and j), and geometric mean diameter of the bed surface sediment (panels e, h and k). Results for the run with uniform sand, i.e., Run 2, are presented in panels a and b. Results for the runs with non-uniform bed material are in panels c-k. In particular, the comparison for Run 4 is in panels c-e, the comparison for Run 6 is in panels f-h, and the comparison for Run 8 is in panels i-k. Vertical dashed blue lines identify the position of the alluvial-bedrock transition. In panels a, c, f and i, black diamonds and grey triangles are

477 respectively experimental water and bed surface elevations, grey and black lines respectively
478 represent the numerical water and bed surface elevations. In panels b, d, g and j, black diamonds
479 and grey lines are respectively experimental and numerical values of alluvial cover. In panels e,
480 h and k, black diamonds and grey lines represent experimental and numerical geometric mean
481 diameter of the bed surface material. Error bars in Figure 7 (panels a, c, f and i) denote 10%
482 error for the water surface elevation and 20% error for bed elevation. Modeled equilibrium bed
483 and water surface elevations are mostly within the error bars and thus in reasonable agreement
484 with the experimental results in the bedrock reaches.

485 The alluvial cover is equal to one in alluvial reaches, i.e. where the bed is entirely
486 covered with sediment, and it is less than one in the bedrock reaches, where the channel bed is
487 partially covered with sediment. Alluvial cover plots (panels b, d, g and j) show that the model
488 is able to reasonably capture the position of the alluvial-bedrock transition. However, the sudden
489 drop in alluvial cover measured in the experiments downstream of the alluvial-bedrock transition
490 is not reproduced in the numerical results. The model only captures measured rates of alluvial
491 cover reduction in the streamwise direction, as shown in Figure 7 with the slopes of regression
492 lines through the numerical results (grey line) and through the experimental points (green dash
493 line). In other words, the grey and the black lines in panels b, d, g and j are nearly parallel
494 showing similar rates of change in alluvial cover in the streamwise direction in the experimental
495 and in the numerical results. The difference between numerical predictions and the experimental
496 results is associated with small-scale phenomena associated with complex flow characteristics
497 that cannot be captured with the proposed formulation. Some of the small-scale phenomena are
498 illustrated in the Supplementary Video showing how flow separation downstream of a bedform,

as well as bedload transport on the model bedrock surface, cause a rapid increase in the fraction of exposed bedrock.

The comparison between predicted and measured geometric mean diameters of the equilibrium bed surface sediment are presented in panels e, h and k. Black diamonds represent experimental points and continuous lines are model predictions. Error bars indicate 5% error and most of the points fall within these bars (except 2 points in run 6 and 2 points in run 8) suggesting a remarkably good agreement between numerical and predicted grain size distributions of the bed surface sediment.

The comparison between numerical and measured grain size distribution (GSD) of the surface material is presented in Figure 8 for samples collected at 0.81 m, 2.81 m and 4.81 m from the test reach entrance. In this figure, black diamonds denote experimental measurements, lines are the model prediction, and error bars indicate 10% variability around the measured data. Results for Run 4 (flow rate of 20 l/s and feed rate of 700 gr/min) are panels a-c. Panels d-f present the comparison between numerical and experimental results for Run 6 (flow rate of 20 l/s and feed rate of 400 gr/min); and the numerical and experimental results for Run 8 (flow rate of 10/s and feed rate of 400 gr/min) are in panels g-i. Figure 8 confirms that the proposed model is able to predict the grain size distribution of the equilibrium bed surface (and thus the bed material fluxes) with errors that are comparable with (if not smaller than) those of one-dimensional models of alluvial morphodynamics [e.g. *Viparelli et al., 2010*; *Viparelli et al.*, 2014].

5 Discussion

The validated model is used herein to investigate 1) spatial changes in equilibrium grains size distribution of the bed surface sediment, flow characteristics and alluvial cover fraction when the bedrock surface slope S_b is steeper than the alluvial equilibrium slope S_o in presence of a stable bedrock-alluvial transition [*Viparelli et al*., 2015]; 2) spatial and temporal changes in the position of a stable alluvial-bedrock transition in response to rising/falling downstream water surface base level; and 3) whether or not the model is able to capture runaway alluviation and initial-condition dependent equilibrium observed in experiments with steep bedrock surfaces by *Chatanantavet and Parker* [2008].

5.1 mixed bedrock-alluvial reach upstream of a bedrock-alluvial transition

A stable bedrock-alluvial transition, i.e., a transition from a bedrock to an alluvial reach, may form when the slope of the bedrock surface S_b is larger than the alluvial equilibrium slope S_o of a river reach subject to the same flow regime and sediment supply. In particular, an equilibrium bedrock-alluvial transition forms when the vertical distance between the downstream bedrock surface and the water level V_d is small enough so that water depth H upstream of the transition is smaller than the sum of the alluvial equilibrium water depth H_o and the minimum thickness of alluvial cover L_{ac}. This is schematically represented in Figure 9 where the black line shows the bedrock surface, the grey line denotes the elevation of the alluvium, the blue line represents the water surface elevation and the dashed grey line represents the minimum thickness for complete alluviation.

In these simulations we use the same flume geometry of the model validation runs; bedrock surface slope S_b = 0.005; bed material, flow rate and feed rate of Run 4, i.e., non-uniform sand, feed rate equal to 700 gr/min and flow rate equal to 20 l/s; downstream water

surface base level ξ_d = 0.17 m corresponding to V_d = 0.17 m, because the datum is located on the model bedrock surface. The minimum thickness of alluvial cover, active layer thickness and flow resistances calculation procedures are the same as those of the model validation runs.

Equilibrium results are presented in Figure 10 where panel a shows equilibrium elevation of the alluvial bed surface (orange line) and of the bedrock (black line). The dashed grey line identifies the minimum thickness of alluvial cover for complete alluviation of the channel bed, the red circle and the dashed green line identify the equilibrium position of the bedrock-alluvial transition. Spatial changes in equilibrium water depth are presented in Figure 10b where the blue line denotes the water depth and the dashed green line identifies the position of the bedrock-alluvial transition. In the bedrock reach upstream of the bedrock-alluvial transition the flow depth increases in the flow direction until it reaches the alluvial equilibrium value H_o at the bedrock-alluvial transition. The water depth remains constant in space and equal to H_o over the alluvial reach.

The spatial increase in flow depth presented in Figure 10b is associated with a streamwise decrease in mean flow velocity and bedload transport capacity of the flow. Recalling that at equilibrium the bedload transport rate is equal to the sediment supply, a spatial decrease in bedload transport capacity must be associated with an increase in alluvial cover p_c, equation (22). The predicted streamwise increase of alluvial cover in the bedrock reach is presented in Figure 10c, where the dashed green line identifies the location of the bedrock-alluvial transition. In the alluvial reach p_c = 1 and the bedload transport rate is everywhere equal to the bedload transport capacity of the flow and to the sediment supply.

The spatial variation of equilibrium geometric mean diameter of bed surface sediment D_{sg} is presented in Figure 10d. In the alluvial reach D_{sg} does not vary in space. In the bedrock reach,

it increases in the flow direction until it reaches its alluvial equilibrium value at the bedrock-alluvial transition. The downstream coarsening of the bed surface sediment in the bedrock reach can be explained considering that, due to the spatial deceleration of the flow, the bed material transport capacity decreases in the flow direction. Consequently, the mobility of coarse grains decreases more than the mobility of fine grains, and the volume fraction content of coarse sediment in the bed surface sediment has to increase to ensure that sediment mass is conserved.

The numerical results of Figure 10 show that when the slope of the bedrock surface is steeper than the alluvial equilibrium slope of a fluvial reach subject to the same flow and sediment supply, flow characteristics of the bedrock reach tend to be characterized by spatial flow deceleration associated with streamwise increase in alluvial cover and formation of a pattern of downstream coarsening of the bed surface sediment. Conversely, when the slope of the bedrock surface is milder than the alluvial equilibrium slope of a river reach subject to the same flow regime and sediment supply (experiments of *Jafarinik et al.* [2019]), the flow hydrodynamics in the bedrock reach is characterized by flow acceleration in the streamwise direction associated with a reduction of alluvial cover and the formation of a pattern of downstream fining of the bed surface sediment.

Due to the lack of predictive models of bedform regime and bedform size in bedrock reaches, spatial changes in bedform geometry have not been predicted. We hypothesize that lower regime bedform height may increase in the streamwise direction upstream of a stable bedrock-alluvial transition. The experiments by *Jafarinik et al.* [2019] suggested that in the case of spatial flow acceleration the bedform regime tend to move from dunes to antidunes with a reduction of the flow resistances associated with form drag. In the case of the spatial flow deceleration observed upstream of a stable bedrock-alluvial transition, we expect to see an

590 increase in dune height associated with an increase in flow depth, reduction in mean flow
591 velocity and increasing flow resistances associated with form drag.
592
593 *5.2 Impacts of sea level rise/fall on alluvial-bedrock transitions*
594 In low-slope bedrock rivers, equilibrium characteristics may be affected by changes in
595 sea level, i.e. the downstream water surface base level ξ_d. Here we use our validated model to
596 study the effects of sea level rise on flow characteristics and sediment transport processes in a
597 mixed bedrock reach characterized by an alluvial-bedrock transition.
598 Input parameters are the sediment size distribution, flow rate and feed rate of Run 4, i.e.
599 20 l/s of flow rate and 700 gr/min of feed rate. We widen the flume from 0.19 m to 1 m to avoid
600 using complicated procedures to remove side wall effects, we elongate the test reach to 30 m and
601 made the bedrock slope steep enough (~ 0.0015) to clearly show the movement of the alluvial-
602 bedrock transition along the reach. In these conditions, the alluvial equilibrium slope S_o is 0.002.
603 Simulations with increasing sea level start with an equilibrium bed. The downstream water
604 surface elevation is then raised in four, 3 mm increments for a total raise of 12 mm. After each
605 increase of downstream water surface elevation, the model is run until new equilibrium
606 conditions are obtained. After each sudden raise in downstream water level, the alluvial-bedrock
607 transition starts to move downstream until it stabilizes.
608 Figure 11 shows the equilibrium elevation of the alluvium for different values of
609 downstream water surface level, the bedrock surface (continuous brown line) and how the stable
610 alluvial-bedrock transition moves downstream following each increase in downstream water
611 surface level. Panels a, b, c in Figure 12 respectively show equilibrium alluvial cover, geometric
612 mean diameter of the surface material (D_{sg}) and water depth. At each location equilibrium water

depth, alluvial cover and D_{sg} increase in response to an increase in the water base level. In Figure 12, the location where the horizontal lines meet the inclined lines are the alluvial-bedrock transition that moves downstream with base level rise.

These results confirm that the alluvial-bedrock transition can move upstream or downstream when sea level rise, subsidence or uplift are present [*Viparelli et al.*, 2015]. We thus expect that in response to base level fall the stable position of an alluvial-bedrock transition will migrate upstream, and at each location of the initial bedrock reach the average fraction of exposed bedrock will increase, the bed surface sediment will become finer and the water depth will be shallower. Similarly, the stable position of a bedrock-alluvial transition in presence of sea level rise is expected to migrate upstream, and at a given location in the initial bedrock reach the alluvial cover will increase in time, the bed surface sediment will coarsen, and the water depth will deepen. In response to base level fall, a stable bedrock-alluvial transition is expected to migrate downstream with consequent reductions of water depth and alluvial cover in the bedrock reach associated with fining of the bed surface sediment.

5.3 Application to steep bedrock reaches

Chatanantavet and Parker [2008] performed experiments with bedrock roughness height of the bedrock surface smaller than the grain roughness of the alluvial patches, i.e., the same condition of the *Jafarinik et al.* [2019] experiments used for model validation. In experiments with bedrock slopes steeper than ~0.005 that commenced with a bare bedrock surface, alluviation of the channel bed was not observed until the sediment feed rate exceeded a threshold value, then rapid deposition of sediment on the channel bed was observed. *Chatanantavet and Parker* [2008] called this rapid deposition of sediment *runaway alluviation*. Further, for bedrock slopes

steeper than ~0.015 *Chatanantavet and Parker* [2008] found that equilibrium was dependent on the initial thickness of alluvium. When the initial thickness of alluvium was smaller than a threshold value, the initial alluvial cover was washed out and equilibrium corresponded to a condition of bare bedrock. If the initial thickness of alluvium was larger than the threshold value, equilibrium conditions with $p_c < 1$ were obtained.

To test the model formulation presented herein on steep bedrock slopes, we tried to model runaway alluviation and initial condition dependent equilibrium. We modified the model to simulate the *Chatanantavet and Parker* [2008] experimental conditions of interest. We considered uniform sediment and we substituted the quasi-steady approximation with a quasi-normal approximation to easily model the *Chatanantavet and Parker* [2008] supercritical flows, i.e. the water depth at each computational node was computed with a Chezy formulation [*Parker et al.*, 2004].

Model results show that the model formulation presented herein is inadequate to reproduce runaway alluviation and the initial-condition dependent equilibrium. We hypothesize that the reason of model failure is in the flow model, which does not track the position of each alluvial and bedrock area. It uses a cross-sectionally averaged roughness height to compute flow resistance and bed shear stresses. This formulation cannot capture the effects of changes in roughness height from alluvial to bedrock patches (and vice versa) on bedload transport. In paragraph 11, *Chatanantavet and Parker* [2008] note that *bare bedrock surfaces were able to accommodate much higher bedload transport rates without alluviation*. A similar sudden change in bedload transport capacity was observed by *Jafarink et al.* [2019] in front of the lee faces of the downstream migrating bedforms, as shown in the Supplementary Video and

discussed above to explain the differences between numerical and experimental cover fractions in Figure 7.

6 Conclusions

We present a novel formulation for the alluvial morphodynamics of bedrock rivers that explicitly accounts for the non-uniformity of the sediment size and for the different roughness between the exposed bedrock and the alluvial patches. Flow resistances are further partitioned between skin friction and form drag to properly account for the presence of small scale bedforms in the sediment transport calculations.

This formulation, implemented in a numerical model, is validated against the experimental results by *Jafarinik et al.* [2019]. The differences between the numerical predictions and the experimental observations in the bedrock reaches are comparable with the differences between numerical and experimental values presented in similar studies on the alluvial morphodynamics of fluvial reaches. Model validation is performed for an equilibrium bedrock reach downstream of an alluvial-bedrock transition, which is characterized by spatial flow acceleration on the bedrock reach associated with a streamwise decrease in the alluvial cover, fining of the bed surface sediment and reduction of bedform height.

Model application to study the alluvial morphodynamics of bedrock reaches upstream of a stable bedrock-alluvial transition reveals that the equilibrium flow on the bedrock reach is characterized by flow deceleration in the downstream direction. This flow deceleration is associated with a streamwise increase of the alluvial cover and the formation of a stable pattern of downstream coarsening of the bed surface sediment to balance the reduction of the bedload

transport capacity. Based on experimental observations, we hypothesize that if dunes form on the alluvial reach, the bedform height in the bedrock reach should increase in the flow direction.

The validated model is also used to study the effects of water surface base level rise/fall on the characteristics and sediment transport processes on low-slope bedrock reaches characterized by an alluvial-bedrock or a bedrock-alluvial transition. The results show that notwithstanding these transitions are stable features of bedrock reaches in equilibrium, their locations can move upstream or downstream in response to changes in water surface base level.

Finally, the model is tested to reproduce runaway alluviation and initial condition dependent equilibrium in steep bedrock reaches [*Chatanantavet and Parker*, 2008], which are due to the differences between bedload transport capacity on the bedrock surface and on the alluvial surface. In the flow model used herein the roughness height used to compute flow resistance and bed shear stress is a cross sectionally average value. The model is thus incapable of reproducing phenomena associated with the different roughness between bedrock and alluvial patches the bedrock and alluvium such as runaway alluviation and initial condition dependent equilibrium.

Acknowledgements

This research was supported by the United States National Science Foundation through award EAR 1250641 and by the University of South Carolina. The model (code transcript in Fortran 95) with proper documentation will soon (i.e. in the second half of February 2020) be made publicly available through the model repository of the Community Surface Dynamics Modeling System (CSDMS).

703

704

705

706

707

NOTATION

C_f Friction coefficient

$C_{f,bs}$ Friction coefficient associated with skin friction

C_{fb} Bed friction coefficient

D_g Geometric mean diameter of the sediment supply

D_i Grain size diameter

D_{90} Grain size such that 90 percent of material are finer

F_i Volume fraction content of sediment in the generic grain size range in the bed surface

f_i Volume fraction content of sediment in the generic grain sizes

f'_i Volume fraction content of sediment in the generic grain size range in the substrate

f_i Volume fraction content of sediment in the generic grain sizes at active-substrate interface

$f_{load,i}$ Volume fraction content of sediment in the generic grain sizes in bedload

Fr Froude number

g Acceleration of gravity

H Water depth

H_o Equilibrium water depth

k_c Composite roughness height

k_{sc} Roughness height associated with skin friction

k_{sa} Roughness height associated with skin friction for alluvium

k_{sb} Roughness height associated with skin friction for bedrock

L_{ac} Minimum thickness of alluvial cover

L_a Active layer thickness in fully alluvial reach

731 $L_a^{'}$ Active layer thickness in bedrock reach

732 $L_{a,av}$ Average active layer thickness

733 p_c Alluvial cover

734 p_b Probability of not having bedrock at elevation z

735 p_{bI} Probability that a point at active-substrate interface is either in alluvium or water

736 q^*_{bi} Nondimensional bedload transport rate per unit width for a generic grain size

737 q_{bi} Bedload transport rate per unit width of the generic grain size

738 q_{bic} Bedload transport capacity of the generic grain size

739 q_{bT} Total (summed over all the grain sizes) bedload transport rate per unit width

740 q_{bTc} Total (summed over all the grain sizes) sediment transport capacity

741 q_w Flow discharge per unit channel width

742 R Submerged specific gravity

743 R_h Hydraulic radius

744 $R_{h,s}$ Hydraulic radius associated with skin friction

745 $R_{h,b}$ Hydraulic radius in the bed region

746 S Bed slope

747 S_b Bedrock slope

748 S_f Friction slope

749 S_o Equilibrium bed slope

750 U Averaged flow velocity

751 η Average elevation of alluvial deposit

752 η_b Bedrock elevation

753 λ_p Bed material porosity

754	ξ_d	Water level at the downstream boundary
755	ρ	Water density
756	σ_g	Geometric standard deviation of the sediment supply
757	τ^*_{bs}	Shields number associated with skin friction
758	τ^*_{bsi}	Shields number associated with skin friction of the generic grain size
759	τ^*_{refi}	Reference Shields number of the generic grain size
760	τ^*_{scg}	Reference value for Shields number
761	V_d	Distance between water level and bedrock surface at downstream
762		
763		
764		
765		
766		
767		

References

Anderson, A. G., Parker, G., & Wood, A. (1975). *The flow and stability characteristics of alluvial river channels*. Project Report 161, University of Minnesota St. Anthony Falls Laboratory.

Blom, A. (2008). Different approaches to handling vertical and streamwise sorting in modeling river morphodynamics. *Water resources research*, 44(3).

Blom, A., Parker, G., Ribberink, J. S., & De Vriend, H. J. (2006). Vertical sorting and the morphodynamics of bed-form-dominated rivers: An equilibrium sorting model. *Journal of Geophysical Research: Earth Surface*, 111(F1). doi: 10.1029/2004JF000175

Blom, A., Viparelli, E., & Chavarrías, V. (2016). The graded alluvial river: Profile concavity and downstream fining. *Geophysical Research Letters*, 43(12), 6285-6293. doi: 10.1002/2016GL068898

Chatanantavet, P., & Parker, G. (2008). Experimental study of bedrock channel alluviation under varied sediment supply and hydraulic conditions. *Water Resources Research*, *44*(12). doi: 10.1029/2007WR006581

Chatanantavet, P., Whipple, K. X., Adams, M. A., & Lamb, M. P. (2013). Experimental study on coarse grain saltation dynamics in bedrock channels. *Journal of Geophysical Research: Earth Surface*, *118*(2), 1161-1176. doi: 10.1002/jgrf.20053

Chaudhry, M. H. (2007). *Open-channel flow*. Springer Science & Business Media.

Chiew, Y. M., & Parker, G. (1994). Incipient sediment motion on non-horizontal slopes. *Journal of Hydraulic Research*, 32(5), 649-660.

De Vries, M. (1965). *Considerations about non-steady bed-load-transport in open channels*. Publication 36, Delft Hydraulics Laboratory, Netherlands.

791 Engelund, F., & Hansen, E. (1967). *A monograph on sediment transport in alluvial streams*.
792 Technical University of Denmark 0stervoldgade 10, Copenhagen K.
793 Gasparini, N. M., Whipple, K. X., & Bras, R. L. (2007). Predictions of steady state and transient
794 landscape morphology using sediment-flux-dependent river incision models. *Journal of*
795 *Geophysical Research: Earth Surface*,*112*(F3). doi: 10.1029/2006JF000567
796 Hodge, R. A., Hoey, T. B., & Sklar, L. S. (2011). Bed load transport in bedrock rivers: The role
797 of sediment cover in grain entrainment, translation, and deposition. *Journal of Geophysical*
798 *Research: Earth Surface*, *116*(F4). doi: 10.1029/2011JF002032
799 Hodge, R., Hoey, T., Maniatis, G., & Leprêtre, E. (2016). Formation and erosion of sediment
800 cover in an experimental bedrock-alluvial channel. *Earth Surface Processes and Landforms*.
801 doi: 10.1002/esp.3924
802 Hoey, T. B., & Ferguson, R. (1994). Numerical simulation of downstream fining by selective
803 transport in gravel bed rivers: Model development and illustration. Water resources research,
804 30(7), 2251-2260.
805 Inoue, T., Izumi, N., Shimizu, Y., & Parker, G. (2014). Interaction among alluvial cover, bed
806 roughness, and incision rate in purely bedrock and alluvial-bedrock channel. *Journal of*
807 *Geophysical Research: Earth Surface*,*119*(10), 2123-2146. doi: 10.1002/2014JF003133
808 Jafarinik, S., Hernández Moreira, R., & Viparelli, E. (2019). Alluvial morphodynamics of
809 bedrock reaches transporting mixed-size sand. Laboratory experiments. *Journal of*
810 *Geophysical Research: Earth Surface* 124, https://doi.org/10.1029/2019JF005058
811 Johnson, J. P. (2014). A surface roughness model for predicting alluvial cover and bed load
812 transport rate in bedrock channels. *Journal of Geophysical Research: Earth Surface*, *119*(10),
813 2147-2173. doi: 10.1002/ 2013JF003000.

814 Lague, D. (2010). Reduction of long-term bedrock incision efficiency by short-term alluvial
815 cover intermittency. *Journal of Geophysical Research: Earth Surface*, *115*(F2). doi:
816 10.1029/2008JF001210
817 Lague, D. (2014). The stream power river incision model: evidence, theory and beyond. *Earth*
818 *Surface Processes and Landforms*, *39*(1), 38-61. doi: 10.1002/esp.3462
819 Lamb, M. P., Dietrich, W. E., & Sklar, L. S. (2008). A model for fluvial bedrock incision by
820 impacting suspended and bed load sediment. *Journal of Geophysical Research: Earth*
821 *Surface*, *113*(F3). doi: 10.1029/2007JF000915
822 Lanzoni, S., & Seminara, G. (2002). Long-term evolution and morphodynamic equilibrium of
823 tidal channels. Journal of Geophysical Research: Oceans, 107(C1), 1-1.
824 Lauer, J. W., Viparelli, E., & Piégay, H. (2016). Morphodynamics and sediment tracers in 1-D
825 (MAST-1D): 1-D sediment transport that includes exchange with an off-channel sediment
826 reservoir. *Advances in Water Resources*, 93, 135-149.
827 Nelson, P. A., & Seminara, G. (2012). A theoretical framework for the morphodynamics of
828 bedrock channels. *Geophysical Research Letters*, 39(6), doi: 10.1029/2011GL050806
829 Nittrouer, J. A., Mohrig, D., Allison, M. A., & Peyret, A. P. B. (2011). The lowermost
830 Mississippi River: a mixed bedrock-alluvial channel *Sedimentology*, *58*(7), 1914-1934. doi:
831 10.1111/j.1365-3091.2011.01245.x
832 Parker, G. (1991a). Selective sorting and abrasion of river gravel. I: Theory. *Journal of*
833 *Hydraulic Engineering*, 117(2), 131-147. doi: 10.1061/(ASCE)0733-9429(1991)117:2(131)
834 Parker, G. (1991b). Selective sorting and abrasion of river gravel. II: Applications. *Journal of*
835 *Hydraulic Engineering*, 117(2), 150-171.

836 Parker, G. (2004). *1D sediment transport morphodynamics with applications to rivers and*
837 *turbidity currents*. E-book available at Gary Parker's Morphodynamics Web Page, last
838 update April, 13, 2006.
839 Parker, G. (2008). Transport of gravel and sediment mixtures. *Sedimentation engineering:*
840 *Processes, measurements, modeling, and practice*, *110*, 165-252. doi:
841 10.1061/9780784408148.ch03.
842 Parker, G. and Klingeman, P.C. (1982), On why gravel bed streams are paved, *Water Resources*
843 *Research*, 18 (5), 1409–1433, 1982.
844 Parker, G., Paola, C., & Leclair, S. (2000). Probabilistic Exner sediment continuity equation for
845 mixtures with no active layer. *Journal of Hydraulic Engineering*, 126(11), 818-826.
846 Shaw, J. B., Mohrig, D., & Whitman, S. K. (2013). The morphology and evolution of channels
847 on the Wax Lake Delta, Louisiana, USA. *Journal of Geophysical Research: Earth Surface*,
848 *118*(3), 1562-1584. doi: 10.1002/jgrf.20123.
849 Shaw, J. B., & Mohrig, D. (2014). The importance of erosion in distributary channel network
850 growth, Wax Lake Delta, Louisiana, USA. *Geology*, 42(1), 31-34.
851 Sklar, L. S., & Dietrich, W. E. (2004). A mechanistic model for river incision into bedrock by
852 saltating bed load. *Water Resources Research*, *40*(6). doi: 10.1029/2003WR002496
853 Tuijnder, A. P., Ribberink, J. S., & Hulscher, S. J. (2009). An experimental study into the
854 geometry of supply-limited dunes. *Sedimentology*, *56*(6), 1713-1727. doi: 10.1111/j.1365-
855 3091.2009.01054.x
856 Turowski, J. M., Lague, D., & Hovius, N. (2007). Cover effect in bedrock abrasion: A new
857 derivation and its implications for the modeling of bedrock channel morphology. *Journal of*
858 *Geophysical Research: Earth Surface*,*112*(F4). doi: 10.1029/2006JF000697

Vanoni, V. A., & Brooks, N. H. (1957). *Laboratory studies of the roughness and suspended load of alluvial streams*. Sedimentation Laboratory California Institute of Technology, Pasadena, California, Report No. E-68.

Viparelli, E., Sequeiros, O. E., Cantelli, A., Wilcock, P. R., & Parker, G. (2010). River morphodynamics with creation/consumption of grain size stratigraphy 2: numerical model. *Journal of Hydraulic Research*, 48(6), 727-741.

Viparelli, E., Gaeuman, D., Wilcock, P., & Parker, G. (2011). A model to predict the evolution of a gravel bed river under an imposed cyclic hydrograph and its application to the Trinity River. *Water Resources Research*, 47(2). doi: 10.1029/2010WR009164

Viparelli, E., Nittrouer, J. A., & Parker, G. (2015). Modeling flow and sediment transport dynamics in the lowermost Mississippi River, Louisiana, USA, with an upstream alluvial-bedrock transition and a downstream bedrock-alluvial transition: Implications for land building using engineered diversions. *Journal of Geophysical Research: Earth Surface*, *120*(3), 534-563. doi: 10.1002/2014JF003257.

Whipple, K. X. (2004). Bedrock rivers and the geomorphology of active orogens. *Annu. Rev. Earth Planet. Sci.*, *32*, 151-185. doi: 10.1146/annurev.earth.32.101802.120356

Whipple, K. X., & Tucker, G. E. (2002). Implications of sediment-flux-dependent river incision models for landscape evolution. *Journal of Geophysical Research: Solid Earth*, 107(B2). doi: 10.1029/2000JB000044

Whipple, K. X., Hancock, G. S., & Anderson, R. S. (2000). River incision into bedrock: Mechanics and relative efficacy of plucking, abrasion, and cavitation. *Geological Society of America Bulletin*, *112*(3), 490-503. doi: 10.1130/0016-7606(2000)112

Wilcock, P. R., & Crowe, J. C. (2003). Surface-based transport model for mixed-size sediment. *Journal of Hydraulic Engineering*, 129(2), 120-128. doi: 10.1061/(ASCE)0733-9429(2003)129:2(120)

Wong, M., Parker, G., DeVries, P., Brown, T. M., & Burges, S. J. (2007). Experiments on dispersion of tracer stones under lower-regime plane-bed equilibrium bed load transport. *Water Resources Research*,*43*(3). doi: 10.1029/2006WR005172

Zhang, L., Parker, G., Stark, C. P., Inoue, T., Viparelli, E., Fu, X., & Izumi, N. (2015). Macro-roughness model of bedrock-alluvial river morphodynamics. *Earth Surface Dynamics*, *3*, 113-138. doi:10.5194/esurf-3-113-2015

List of Tables

List of Figures

the surface material. The black lines represent the perfect agreement between experimental and numerical results. The dashed lines depict the errors around the perfect match.

Figure 7. Experimental and numerical comparison of water (ζ) and bed surface (η) elevation, alluvial cover and geometric mean diameter of the surface material in Runs 2, 4, 6 and 8. The points are experimental data and the solid lines are the numerical results. The blue dashed line represents the location of alluvial-bedrock transition and the green dashed line denote the linear regression of the experimental alluvial cover on the bedrock reach.

Figure 8. Comparison between experimental and numerical grain size distributions of bed surface material at 0.81 m (upstream), 2.81 m (middle) and 4.81 m (downstream) from the test reach entrance. Grey lines represent numerical resuts and the diamonds denote the experimental data. Vertical bars denote 10% error

Figure 9. Schematic plot of a bedrock reach upstream of the bedrock-alluvial transition.

Figure 10. Numerical results with a stable bedrock-alluvial transition. a) bed surface (orange line), bedrock elevation (black line) and the minimum thickness of alluvial cover (dashed grey line). Red circle indicates the bedrock-alluvial transition. b) water depth. c) alluvial cover. D) the geometric mean diameter of the surface sediment. The green dashed lines represent the bedrock-alluvial transition

Figure 11. Location of stable alluvial-bedrock transition for base level rise. Brown solid and dashed lines represent the bedrock surface and the minimum thickness for fully alluviation respectively. The dark blue, yellow, green, light blue and purple lines are bed surface elevations after 0, 3, 6, 9 and 12 mm of base level rise.

Figure 12. (a) Equilibrium water depth, (b) Geometric mean diameter of surface material and (c) the alluvial cover . Dark blue, yellow, green, light blue and purple respectively represent the initial equilibrium bed and equilibrium results after 3 mm, 6 mm, 9 mm and 12 mm base level rise.

946 Table 1. Experimental conditions for the model validation runs [*Jafarinik et al.*, 2019]. ξ_d denotes

947 the downstream water surface base level and H_o the alluvial equilibrium flow depth

Run	Flow Rate (L/s)	Feed Rate (gr/min)	ξ_d (m)	Ho (m)	Grain Size	Condition
1	20	700	0.224	0.176	Uniform	Fully alluvial
2	20	700	0.160		Uniform	Exposed bedrock
3	20	700	0.223	0.172	Nonuniform	Fully alluvial
4	20	700	0.154		Nonuniform	Exposed bedrock
5	20	400	0.225	0.186	Nonuniform	Fully alluvial
6	20	400	0.186		Nonuniform	Exposed bedrock
7	10	400	0.146	0.086	Nonuniform	Fully alluvial
8	10	400	0.083		Nonuniform	Exposed bedrock

948

949

950

951

952

953

954

955

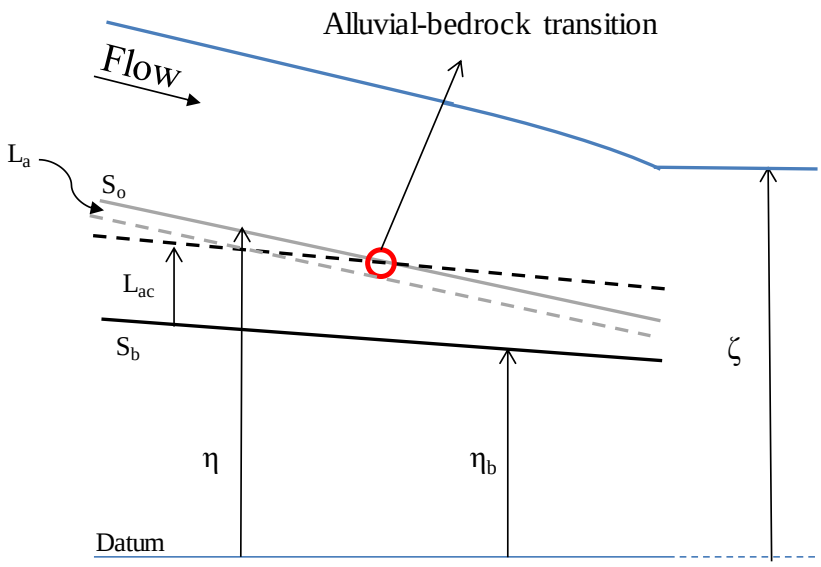

Figure 1. Schematic geometry of the model domain. Black solid line is the bedrock surface. Grey line is the bed surface and blue thick line represents the water surface. The red circle shows the alluvial-bedrock transition. The dashed grey line denotes the active layer (L_a) thickness and the dashed black line represents the minimum thickness of alluvial cover (L_{ac}).

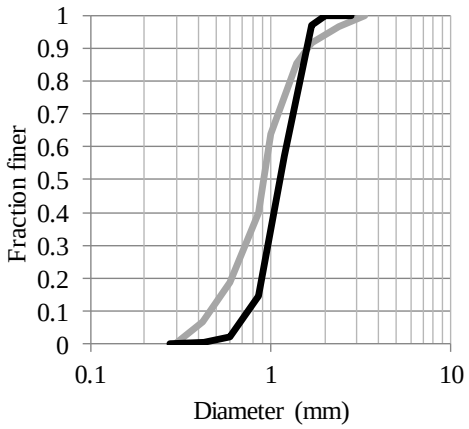

Figure 2. Grain size distribution of the bedload material. Grey dashed line shows the GSD of uniform material used in Run 1 and Run 2. Black solid line represents the GSD of non-uniform material used in Runs 3-8.

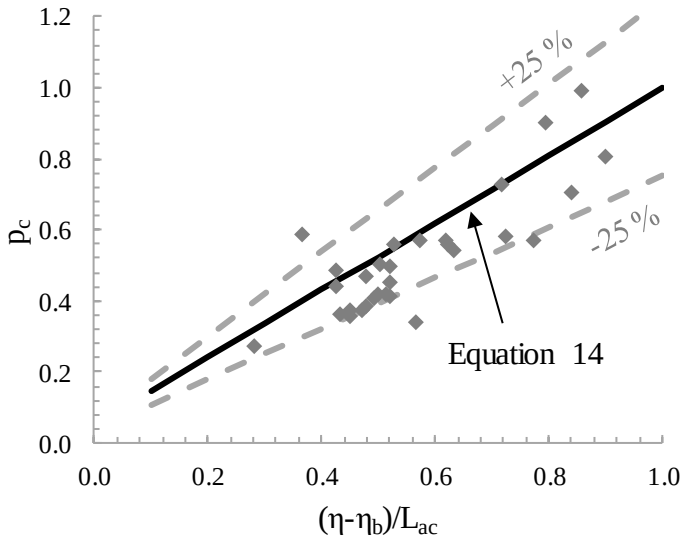

969
970 Figure 3. Alluvial cover formulation of *Viparelli et al.* [2015] vs experimental data. Grey
971 diamonds are experimental points, the black line is equation (17) and the dashed lines indicate
972 ±25% around the predicted value.

973

974

975

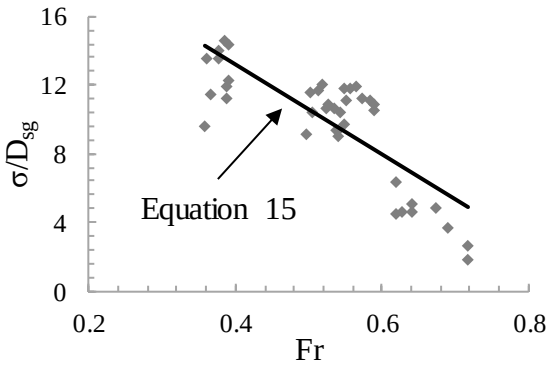

Figure 4. Flow resistance closures based on the experimental data. Dimensionless standard deviation of bed elevation fluctuation against Froude number. Grey diamonds represent the experimental points and the lines represent regression line.

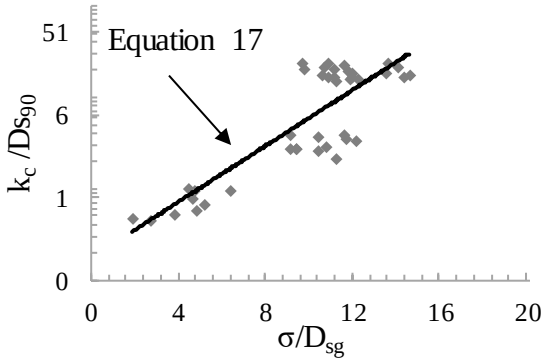

Figure 5. Dimensionless composite roughness height against dimensionless standard deviation of bed elevation fluctuation. Grey diamonds represent the experimental points and the lines represent regression line.

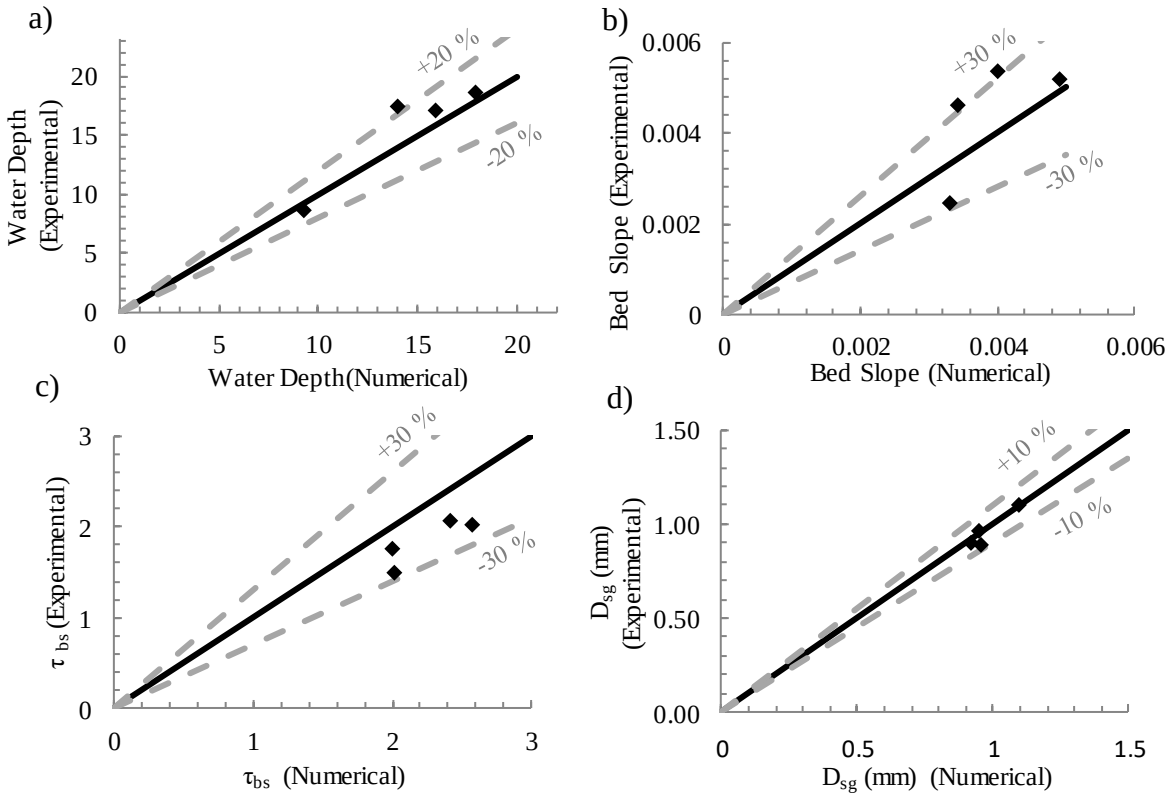

Figure 6. Comparison of experimental and numerical results for the fully alluvial runs. a) Water depth, b) bed slope, c) shear stress associated with skin friction, d) geometric mean diameter of the surface material. The black lines represent the perfect agreement between experimental and numerical results. The dashed lines depict the errors around the perfect match.

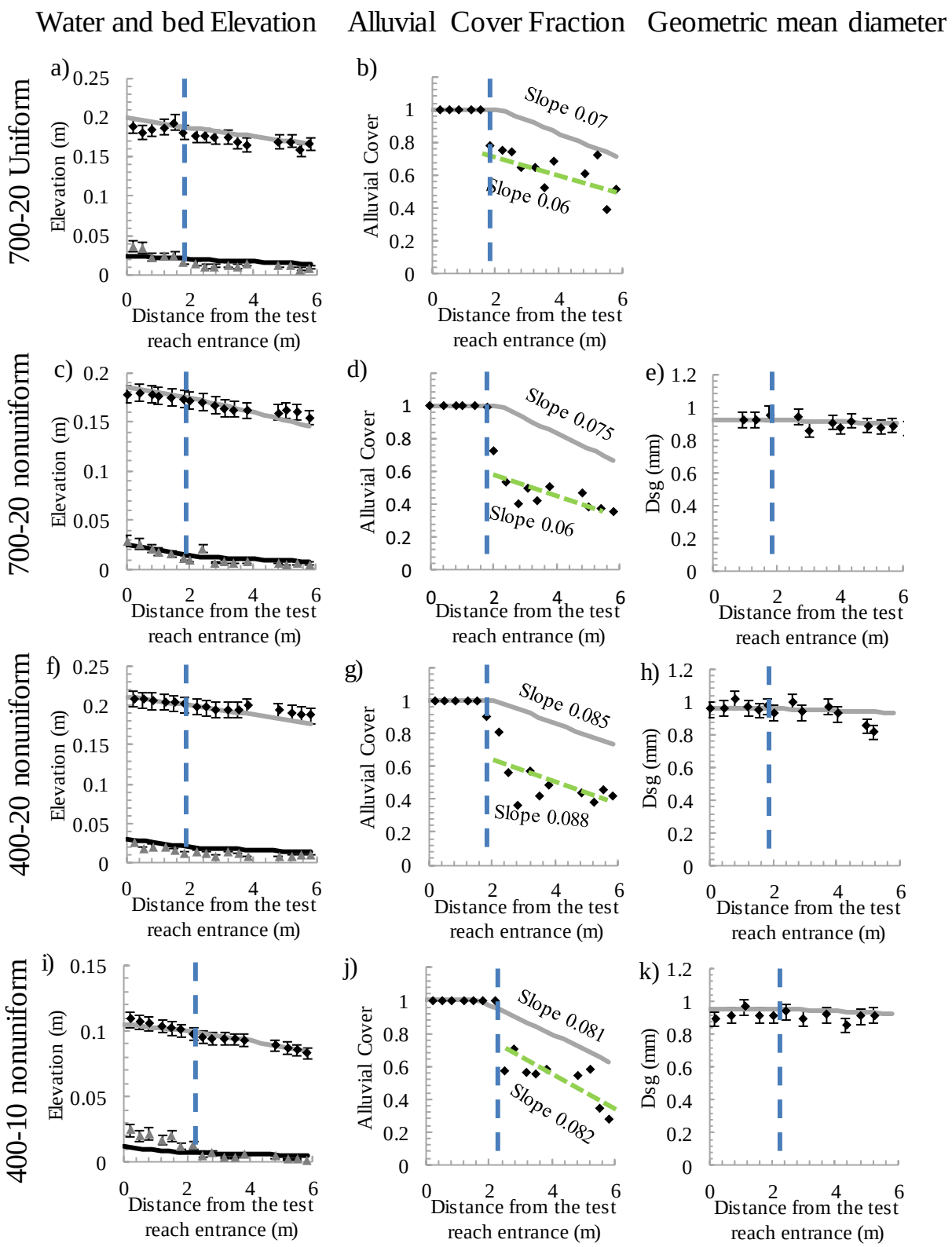

Figure 7. Experimental and numerical comparison of water (ζ) and bed surface (η) elevation, alluvial cover and geometric mean diameter of the surface material in Runs 2, 4, 6 and 8. The

1000 points are experimental data and the solid lines are the numerical results. The blue dashed line
1001 represents the location of alluvial-bedrock transition and the green dashed line denote the linear
1002 regression of the experimental alluvial cover on the bedrock reach.

1003

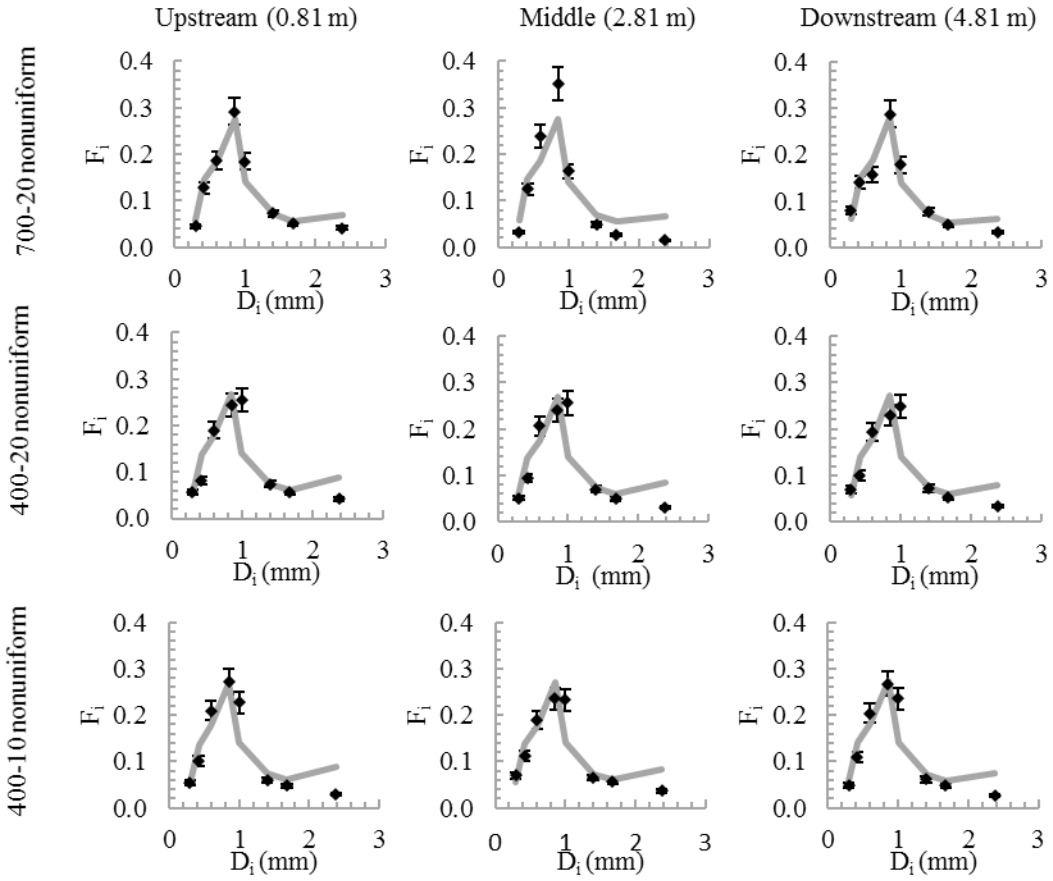

Figure 8. Comparison between experimental and numerical grain size distributions of bed surface material at 0.81 m (upstream), 2.81 m (middle) and 4.81 m (downstream) from the test reach entrance. Grey lines represent numerical results and the diamonds denote the experimental data. Vertical bars denote 10% error.

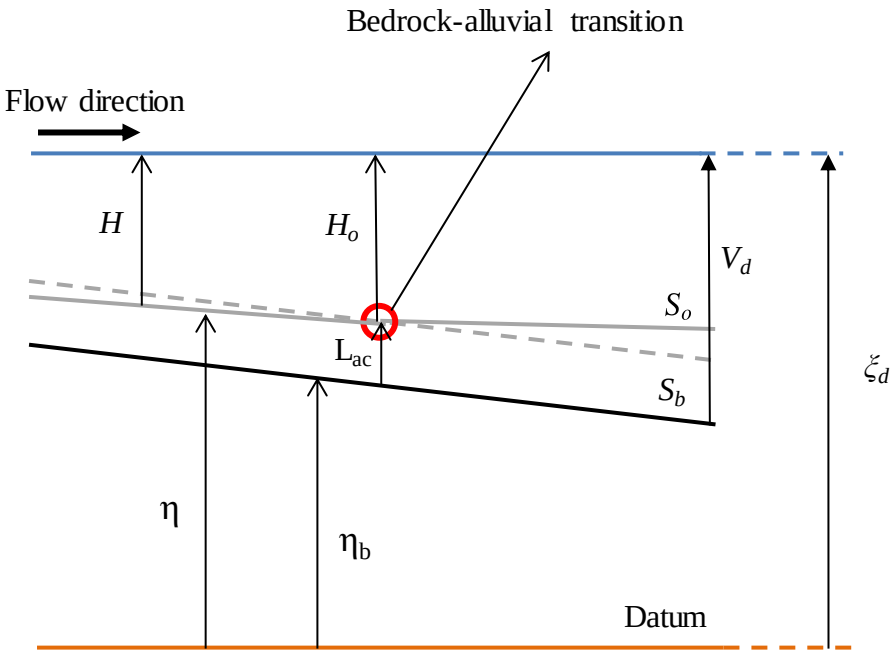

Figure 9. Schematic plot of a bedrock reach upstream of a bedrock-alluvial transition.

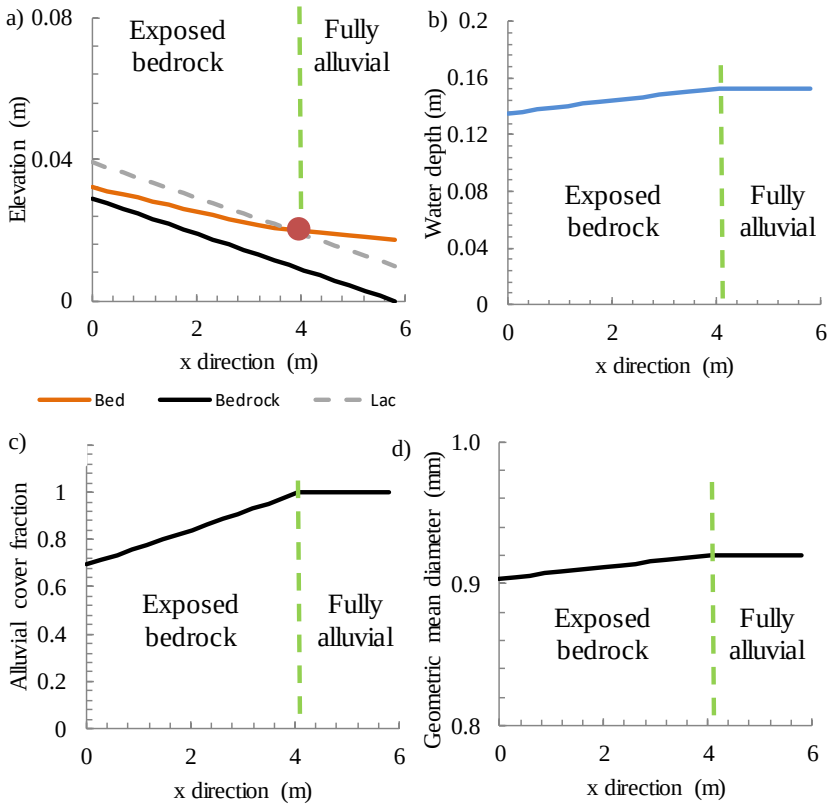

Figure 10. Numerical results with a stable bedrock-alluvial transition. a) bed surface (orange line), bedrock elevation (black line) and the minimum thickness of alluvial cover (dashed grey line). Red circle indicates the bedrock-alluvial transition. b) water depth. c) alluvial cover. D) the geometric mean diameter of the surface sediment. The green dashed lines represent the bedrock-alluvial transition

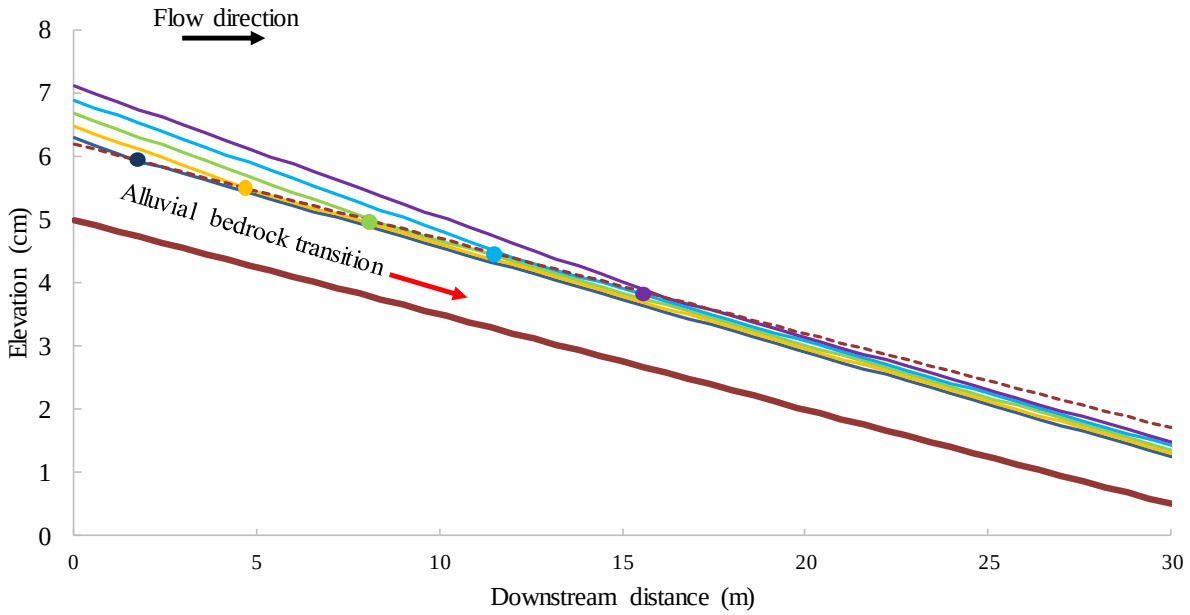

Figure 11. Location of stable alluvial-bedrock transition for base level rise. Brown solid and dashed lines represent the bedrock surface and the minimum thickness for fully alluviation respectively. Dark blue, yellow, green, light blue and purple respectively represent the initial equilibrium bed and equilibrium results after 3 mm, 6 mm, 9 mm and 12 mm base level rise.

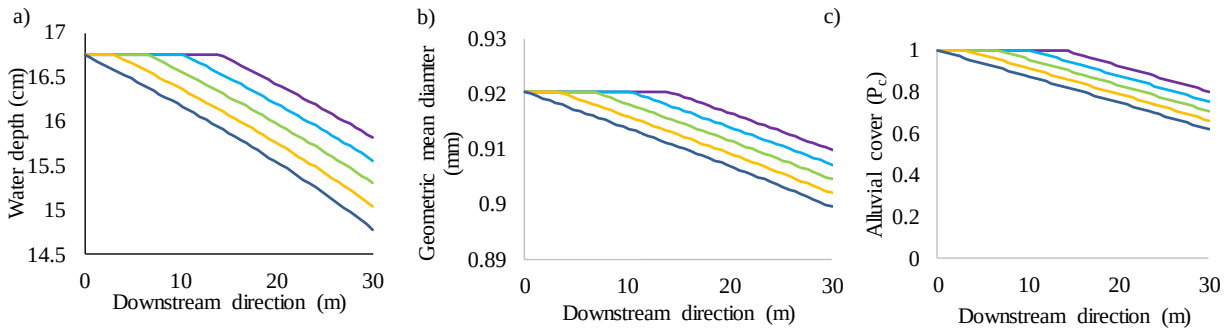

Figure 12. (a) Equilibrium water depth, (b) Geometric mean diameter of surface material and (c) the alluvial cover. Dark blue, yellow, green, light blue and purple respectively represent the initial equilibrium bed and equilibrium results after 3 mm, 6 mm, 9 mm and 12 mm base level rise.